

RESEARCH ARTICLE | MARCH 04 2024

Transport cross sections and collision integrals for $N(^4S)-O(^3P)$ and $N(^4S)-O(^1D)$ interactions in high-temperature air plasmas

Special Collection: [K. R. Sreenivasan: A Tribute on the occasion of his 75th Birthday](#)

Zi Ding (丁子) ; Zhi Qin (秦智)  ; Linhua Liu (刘林华) 



Physics of Fluids 36, 037105 (2024)

<https://doi.org/10.1063/5.0190853>



CrossMark



Physics of Fluids

Special Topic:
Selected Papers from the 2023 Non-Newtonian
Fluid Mechanics Symposium in China

Submit Today



Transport cross sections and collision integrals for $N(^4S)-O(^3P)$ and $N(^4S)-O(^1D)$ interactions in high-temperature air plasmas

Cite as: Phys. Fluids **36**, 037105 (2024); doi: 10.1063/5.0190853

Submitted: 9 December 2023 · Accepted: 16 February 2024 ·

Published Online: 4 March 2024



View Online



Export Citation



CrossMark

Zi Ding (丁子),^{1,2} Zhi Qin (秦智),^{1,2,a)} and Linhua Liu (刘林华)^{1,2,3,b)}

AFFILIATIONS

¹School of Energy and Power Engineering, Shandong University, Jinan 250061, China

²Optics & Thermal Radiation Research Center, Institute of Frontier and Interdisciplinary Science, Shandong University, Qingdao 266237, China

³School of Energy Science and Engineering, Harbin Institute of Technology, Harbin 150001, China

Note: This paper is part of the special topic, K. R. Sreenivasan: A Tribute on the occasion of his 75th Birthday.

^{a)}Author to whom correspondence should be addressed: z.qin@sdu.edu.cn

^{b)}Electronic mail: liulinhua@sdu.edu.cn

ABSTRACT

Collisions between nitrogen (N) and oxygen (O) play a crucial role in determining transport coefficients in high-temperature atmospheres of Earth and planetary. In this study, the momentum transfer, viscosity, third-moment, and fourth-moment transport cross sections for the $N(^4S)-O(^3P)$ and $N(^4S)-O(^1D)$ interactions are reported in the collision energy range of 10^{-6} –10 Hartree based on the classical and semiclassical methods. The new and accurate potential energy curves for N–O interactions, which are used to provide the input for calculations of the cross sections, are calculated based on the state-of-the-art *ab initio* method. The classical and semiclassical collision integrals are provided at 300–50 000 K, and the results support the calculation of transport coefficients in a third-order approximation. In particular, the collision data for the $N(^4S)-O(^1D)$ interaction based on *ab initio* points are reported for the first time. The calculated transport cross sections and collision integrals are helpful for studies of modeling the high-temperature air plasmas.

Published under an exclusive license by AIP Publishing. <https://doi.org/10.1063/5.0190853>

I. INTRODUCTION

Accurate transport properties for high-temperature air plasmas are crucial for computational fluid dynamics (CFD) modeling in various applications, including machining, metallurgy, material preparation, and aerospace.^{1–3} According to the Chapman–Enskog theory,^{4,5} transport coefficients can be expressed in the form of collision integrals. In high-temperature air plasmas, particularly for the hypersonic flow, the temperature in the forward regions of the vehicle or meteoroid is sufficiently high to cause dissociation of N_2 and O_2 , resulting in the presence of numerous N and O atoms in these regions.^{6–8} Nitrogen and oxygen are the most abundant elements in the Earth’s atmosphere, and the collision between them is crucial and cannot be neglected in modeling the transport properties of high-temperature air plasmas.⁹

In addition to the Earth’s atmosphere, N and O atoms also exist in the atmospheres of other planets, such as the atmospheres of Venus and Mars.^{10,11} During the Astro-2 space shuttle mission, the Hopkins Ultraviolet Telescope obtained the far-ultraviolet spectra of Venus and

Mars in the wavelength range of 820–1840 Å at 4 Å resolution. Feldman *et al.*¹² observed O I and N I emissions of Venus and Mars using these data. In the upper atmospheres of Mars and Venus, N and O atoms are generated from extreme UV photodissociation of O_2 , CO_2 , and N_2 in the dayside upper atmosphere and transported to the night side.^{13,14} Moreover, atomic nitrogen occupies a central position in the chemistry of the upper atmosphere of Mars.^{15,16} The dayside upper atmosphere has a much higher density than the nightside one on both Venus and Mars. This density gradient horizontal advection and subsolar to antisolar circulation transport results in a dayside-to-nightside gas flow, which contains light species such as H, He, N, and O. Especially for Venus’ southern hemisphere clouds, the cloud-top winds can reach 105 m/s,¹⁷ which can increase the collision processes between particles. The study of collision between N and O is helpful for understanding the transport properties of planetary atmospheres.^{18–20}

According to the Chapman–Enskog theory,^{4,5} collision integrals are the foundation for calculating the transport properties. The first

step in calculating the collision integrals is to obtain the potential energy curves (PECs) required to describe the collision process. The accuracy of the interatomic interaction potential significantly affects the reliability of the collision integrals.^{21,22} In previous works, Capitelli *et al.*,^{23,24} Sourd *et al.*,²⁵ Laricchiuta *et al.*,²⁶ and Su *et al.*²⁷ employed analytical potential energy functions, such as the phenomenological, Lennard-Jones, Murrell-Sorbie, Hulbert-Hirschfelder, and repulsive exponential potentials, to calculate the collision integrals for the N-O interactions. However, these functions can only accurately produce the potential wells of PECs, which cannot guarantee the accuracy of PECs at both short- and long-internuclear distances. Buchowiecki *et al.*²² investigated the collision integrals for N-H interactions by employing various analytical PECs and concluded that the deviation of collision integrals from various analytical functions could exceed 10% at low temperatures. Recent studies²⁸⁻³⁰ showed that using state-of-the-art *ab initio* calculations as well as reliable fitting functions can provide theoretically reasonable potential energy points for both short and long internuclear distances, thus generating reliable collision integrals.

In previous studies, both the classical method^{23,25-27} and the semiclassical method^{9,31} have been employed to calculate the collision integrals for N-O interactions. Although many studies analyzed low collision energy cross sections using the semiclassical method,³² the difference between the results calculated by these two methods for N-O interaction has not been investigated. Moreover, most previous studies^{9,23,25-27,31} only focused on collision between ground state N(⁴S) and ground state O(³P). In the high-temperature air plasma flow field, N and O in multiple electronic states, including N(⁴S), N(²D), N(²P), O(³P), and O(¹D), may exist. At around 4000 K, oxygen is nearly completely dissociated, while nitrogen is just beginning to dissociate. According to the statistical mechanism, the probability of the interaction between O(³P) and O(¹D) with N(⁴S) is higher compared to those of interactions between N and O with other electronic states at high temperatures. The N(⁴S)-O(¹D) interaction should be considered. Furthermore, the high-order approximations are crucial in describing transport properties in the ionization regime. According to Hirschfelder *et al.*,⁴ the calculation of third-order transport coefficients such as viscosity and thermal conductivity of pure gases requires collision integrals of order (4,4). However, most previous studies^{9,23,25,27,31} have only provided collision integrals up to order (3,3), and only a few studies²⁶ reported collision integrals up to order (4,4) based on the phenomenological approach.

Taking above into consideration, we first report the new and accurate PECs for N(⁴S)-O(³P) and N(⁴S)-O(¹D) interactions based on the high-accuracy *ab initio* method. Subsequently, we calculate accurate transport cross sections using the classical and semiclassical methods in the collision energy range of 10⁻⁶-10 Hartree, including the momentum transfer, viscosity, third-moment, and fourth-moment cross sections. We analyze the differences in transport cross sections determined by the classical method and semiclassical method, with a specific focus on collision effects at low collision energies. Finally, we report the classical and semiclassical collision integrals at 300-50 000 K and provide the fitting functions of these collision integrals.

II. METHODOLOGY

A. Collision integrals

For the classical mechanics,⁴ the transport cross section can be expressed by the impact parameter *b* as follows:

$$Q^{(n)}(E) = 2\pi \int_0^\infty b \{1 - \cos^l[\chi(b, E)]\} db \quad (1)$$

and the deflection angle χ can be calculated by

$$\chi(b, E) = \pi - 2b \int_{r_c}^\infty \frac{dr}{r^2 \sqrt{1 - \frac{b^2}{r^2} - \frac{V(r)}{E}}}, \quad (2)$$

where *r* is the internuclear distance and *V*(*r*) is the PEC. The lower limit of integration *r_c* is defined as the distance of the closest approach depending on *b* and relative collision energy *E*.

For the semiclassical method, the transport cross section can be expressed in terms of the scattering phase shift η_l based on the quantum theory. The η_l can be defined by the Wentzel-Kramers-Brillouin (WKB) approximation as³³

$$\eta_l = k \left\{ \int_{r_x}^\infty [G(r)]^{1/2} dr - \int_b^\infty \left[1 - \left(\frac{l+1}{kr} \right)^2 \right]^{1/2} dr \right\}, \quad (3)$$

where *k* is the wave number ($k = \sqrt{2\mu E}$, μ is the reduced mass of the ion-parent-atom interaction collision system), *l* is the angular momentum quantum number, and the lower limit of the integral *r_x* is the largest root of the following equation:

$$G(r) \equiv 1 - \frac{V(r)}{E} - \frac{b^2}{r^2} = 0, \quad (4)$$

where *b* equals to $(l + 1/2)/k$, which can be determined by the classical impact parameter.⁹

The momentum transfer (MTCS), viscosity (VCS), third-moment (TCS), and fourth-moment (FCS) cross sections for the semiclassical method can be calculated by^{34,35}

$$Q^{(n)}(E) = \frac{4\pi}{k^2} \sum_\nu^n \sum_{l=0}^\infty a_{n\nu}^l \sin^2(\eta_{l+\nu} - \eta_l), \quad (5)$$

where the values of ν are odd or even according to the odd or even parity of *n*. The coefficients $a_{n\nu}^l$ can be determined by recursion from⁹

$$(2l + 1)x^n P_l(x) = \sum_{v=-n}^n a_{nv}^l P_{l+v}(x), \quad (6)$$

where $P_l(x)$ is the Legendre polynomial. The specific expressions for the first four-moment transport cross sections are given in the Appendix.

According to the Chapman-Enskog theory,^{4,5} the average reduced collision integrals can be calculated by

$$\sigma^2 \Omega^{(n,s)*} = \frac{F(n,s)}{2(k_B T)^{s+2}} \int_0^\infty e^{-E/(k_B T)} E^{s+1} \bar{Q}^n(E) dE, \quad (7)$$

where (*n,s*) is the order of collision integral, *k_B* is Boltzmann constant, *T* is the temperature, $\bar{Q}^n(E)$ is the mean transport cross section and is obtained by the weighted average of cross sections corresponding to each of electronic states,³⁶ and *F*(*n,s*) is the scale factor and can be obtained from the following relation:³⁷

$$F(n,s) = \frac{4(n+1)}{\pi(s+1)! [2n+1 - (-1)^n]}. \quad (8)$$

TABLE I. The weighting factors for the calculation of mean transport cross section.

Collision process	State	Weight
N(⁴ S)–O(³ P)	² Π	4/36
	² Σ ⁺	2/36
	⁴ Π	8/36
	⁴ Σ ⁺	4/36
	⁶ Π	12/36
	⁶ Σ ⁺	6/36
N(⁴ S)–O(¹ D)	⁴ Σ [−]	4/20
	⁴ Π	8/20
	⁴ Δ	8/20

The mean cross sections of multipotential interaction are the average of the different potentials, and its statistical weight is equal to the spin multipotential interaction for Σ states and two times the spin multipotential interaction for Π and Δ states.^{23,38} Table I presents the weighting factors for calculating the mean transport cross sections for N(⁴S)–O(³P) and N(⁴S)–O(¹D) interactions.

B. *Ab initio* calculations of potential energy curves

In this work, the MOLPRO 2015 program package^{39–41} was employed for calculating PECs corresponding to N(⁴S)–O(³P) and N(⁴S)–O(¹D) interactions. First, our calculations employ the Hartree–Fock and the state-averaged complete active space self-consistent field (CASSCF) methods to obtain the wave function of the electronic states, followed by the internally contracted multireference configuration interaction method with the Davidson correction (icMRCI+Q).⁴² We adopt the aug-cc-pV6Z (AV6Z) basis set^{43–45} to describe nitrogen and oxygen atoms. MOLPRO is unable to take advantage of the $C_{\infty v}$ symmetry, the $C_{\infty v}$ molecules must be treated in the corresponding subgroup. For instance, NO, which belongs to the $C_{\infty v}$ symmetry, is replaced by its maximum Abelian C_{2v} subgroup. The reducing map of irreducible representations from $C_{\infty v}$ to C_{2v} is $\Sigma^+ \rightarrow A_1$, $\Pi, \Phi \rightarrow B_1$, $\Pi, \Phi \rightarrow B_2$, and $\Sigma^- \rightarrow A_2$. For CASSCF and MRCI calculations, 12 molecular orbitals were put into the active space and 2 molecular orbitals were put into the closed space for the N(⁴S)–O(³P) interaction.

In order to improve the accuracy of highly adiabatic excited state calculations, 14 active molecular orbitals and 2 closed orbitals were considered for the N(⁴S)–O(¹D) interaction.

A total of nine electronic states (i.e., X ²Π, A ²Σ⁺, a ⁴Π, b ⁴Σ⁺, c ⁶Π, d ⁶Σ⁺, 1 ⁴Σ[−], 2 ⁴Π, and 3 ⁴Δ states) that are relevant to the dissociation limit of N(⁴S)–O(³P) and N(⁴S)–O(¹D) were considered. The PECs of these electronic states are shown in Fig. 1. The very short range interaction affects the high temperature behavior of collision integrals.²² The collision integral at 50 000 K corresponds to an average translational energy of approximately 6.5 eV; however, the calculations must account for particles with at least a few times larger energy. It means that the reliable calculations of the collision integrals in the considered temperature range must be based on PECs extending in the short-range region to energies of 30–50 eV. To ensure the accuracy of collision integrals within the temperature range considered, our calculated potential energy points cover a broader internuclear range (1.1–2.6 Hartree or 29.9–70.7 eV) compared to previous theoretical studies^{31,46} (see the supplementary material for details). Additionally, *ab initio* methods are not suitable for calculating potential energies at very small internuclear distances. Considering this limitation, we extrapolated the potential energy points using an exponential form (i.e., $a + be^{-cr}$, where a , b , and c are the fitting parameters) at short internuclear distances (10^{-6} – 0.7 Å) based on LEVEL 8.0.⁴⁷ Furthermore, the cubic spline interpolation method was used to fit potential energy points for the calculation of transport cross sections. The total root mean square errors of cubic spline interpolation functions to *ab initio* potential energy points for N(⁴S)–O(³P) and N(⁴S)–O(¹D) interactions do not exceed 10^{-9} cm^{−1}.

III. ANALYSIS OF RESULTS

In order to verify the reliability of our calculated *ab initio* potential energy points, we compared PECs of the X ²Π, a ⁴Π, 1 ⁴Σ[−], and A ²Σ⁺ electronic states with those of previous studies,^{31,46} as shown in Fig. 2. Our PECs, represented by solid lines, were calculated using the icMRCI+Q method with the aug-cc-pV6Z basis set. The PECs calculated by Levin *et al.*,³¹ which used the MRCI+Q method with the DZP Gauss basis set and extrapolation for the short-range repulsive region, are illustrated by double-dot lines. The dashed lines represent PECs from Zammit *et al.*,⁴⁶ who adopted the MRCI+Q method with the aug-cc-pwCVQZ basis set. Our PECs for the X ²Π, a ⁴Π, and

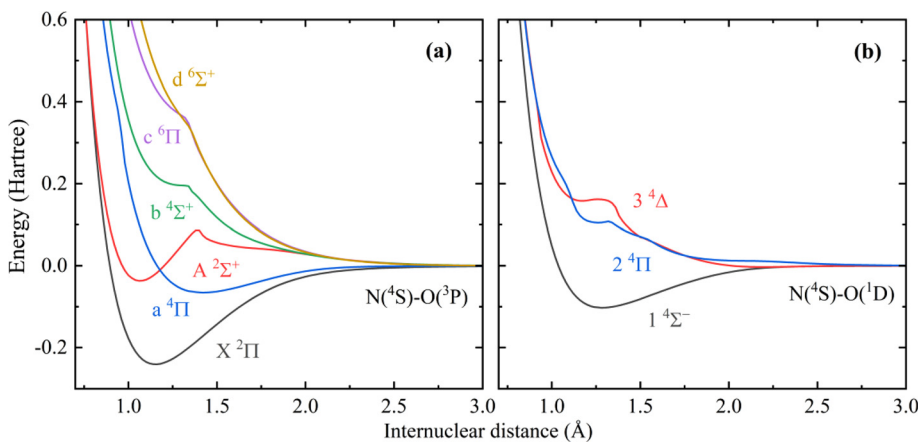


FIG. 1. Potential energy curves for the electronic states corresponding to (a) N(⁴S)–O(³P) and (b) N(⁴S)–O(¹D) interactions.

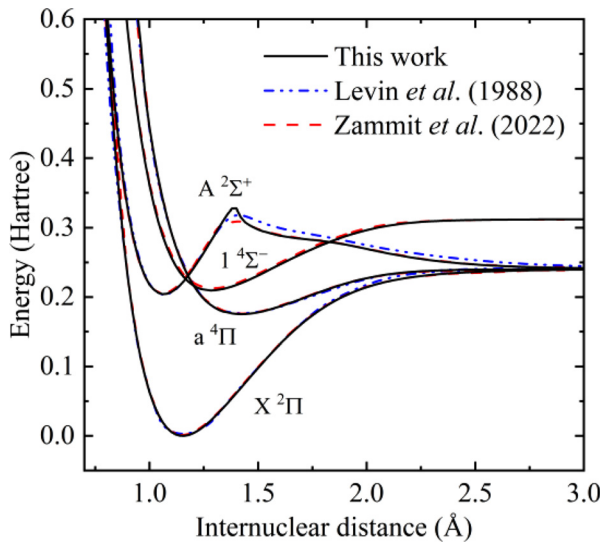


FIG. 2. Comparison of PECs of $X^2\Pi$, $a^4\Pi$, $1^4\Sigma^-$, and $A^2\Sigma^+$ states corresponding to N–O interactions with those from Levin *et al.*³¹ and Zammit *et al.*⁴⁶

$1^4\Sigma^-$ electronic states are in excellent agreement with previous studies. For the $A^2\Sigma^+$ electronic state, our results are different from those of Levin *et al.*³¹ and Zammit *et al.*⁴⁶ at internuclear distances near 1.4 Å. Our results and those of Zammit *et al.*⁴⁶ are slightly smaller than those of Levin *et al.*³¹ for internuclear distances larger than 1.4 Å. Overall, our *ab initio* potential energy points for $N(^4S)-O(^3P)$ and $N(^4S)-O(^1D)$ interactions are reliable.

Figure 3 displays the transport cross sections of MTCs, VCSs, TCSs, and FCSs for the $N(^4S)-O(^3P)$ interaction obtained by classical and semiclassical methods. To accurately calculate the semiclassical cross sections, the angular momentum quantum number l was accumulated up to 10 000, ensuring a decimal accuracy of five significant figures. As shown in Fig. 3, the transport cross sections obtained by the semiclassical method exhibit obvious oscillations at collision energies below about 3×10^{-4} Hartree. This behavior can be attributed to the inclusion of wavelike properties of particles and quantum mechanical effects in the semiclassical method, in contrast to the classical method that assumes particles have well-defined positions and momenta. Figure 4 presents the deviation between the first four-moment transport cross sections for the $N(^4S)-O(^3P)$ interaction based on classical and semiclassical methods. The oscillation of transport cross sections induced by the quantum effect gradually diminishes with increasing

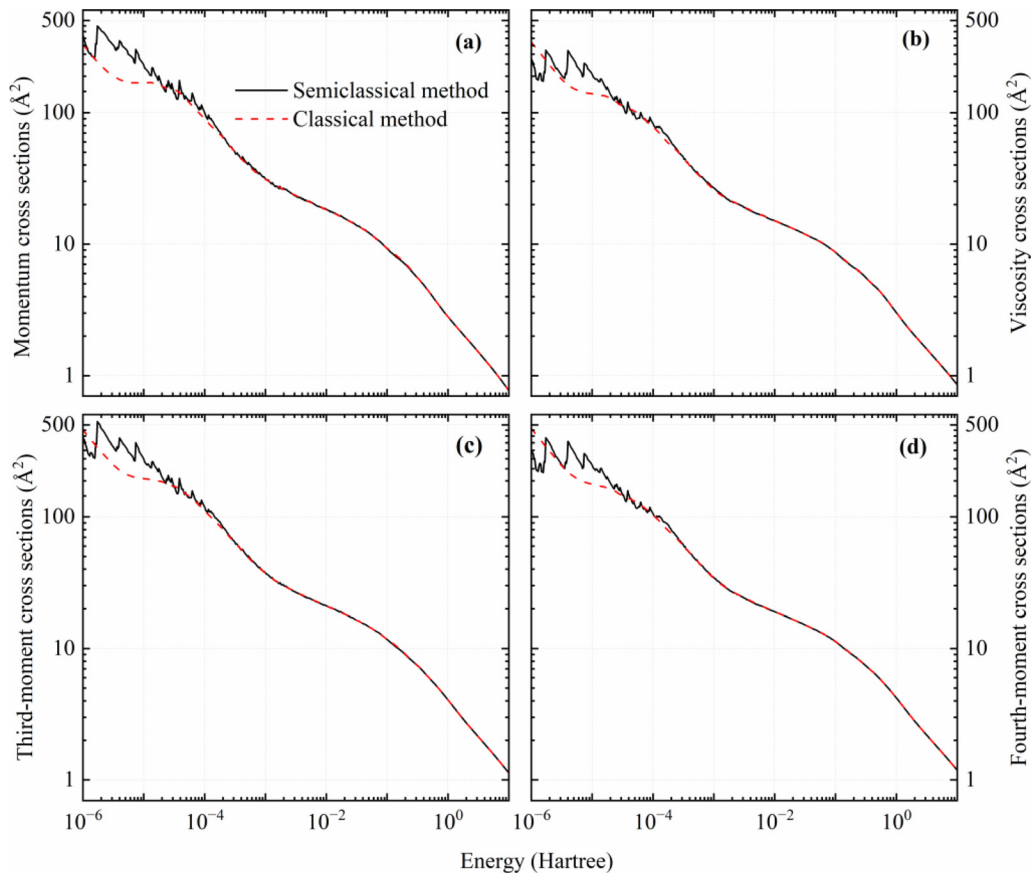


FIG. 3. Transport cross sections including (a) momentum transfer, (b) viscosity, (c) third-moment, and (d) fourth-moment cross sections for the $N(^4S)-O(^3P)$ interaction obtained by semiclassical method and classical method.

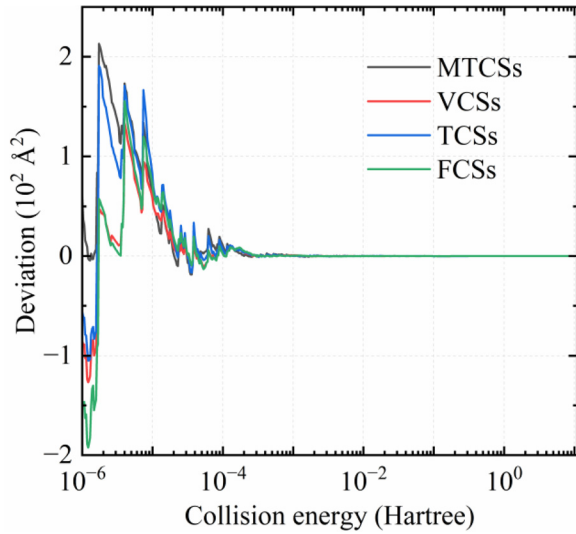


FIG. 4. The deviations between momentum transfer, viscosity, the third-moment, and the fourth-moment cross sections for $N(^4S)-O(^3P)$ interaction obtained by the classical and semiclassical methods.

collision energies, and the deviation becomes negligible at high collision energies ($>3 \times 10^{-4}$ Hartree). The deviations of transport cross sections are also influenced by the number of electronic states and their statistical weights correlating to their dissociation limits.

Figure 5 illustrates the transport cross sections of MTCSSs, VCSs, TCSs, and FCSs for the $N(^4S)-O(^1D)$ interaction obtained by the classical and semiclassical methods. At collision energies above 5×10^{-2} Hartree, the transport cross sections obtained by classical and semiclassical methods are nearly identical. The semiclassical cross sections for $N(^4S)-O(^1D)$ interaction exhibit continuous oscillations at collision energies smaller than 10^{-4} Hartree due to the quantum effect. The details of the MTCSSs, VCSs, TCSs, and FCSs cross sections for $N(^4S)-O(^3P)$ and $N(^4S)-O(^1D)$ interactions are available in the supplementary material.

Tables II and III provide a comparison of collision integrals $\sigma^2\Omega^{(1,1)*}$ and $\sigma^2\Omega^{(2,2)*}$ for $N(^4S)-O(^3P)$ interaction with previous theoretical results.^{9,23,48,49} Levin *et al.*⁹ calculated the collision integrals using the semiclassical method based on the *ab initio* points. In contrast, Capitelli *et al.*,²³ Yun *et al.*,⁴⁸ and Laricchiuta *et al.*⁴⁹ used the classical method with fitting potential energy functions to calculate the collision integrals. For the collision integrals $\sigma^2\Omega^{(1,1)*}$, our predicted theoretical results, which were obtained by classical and semiclassical

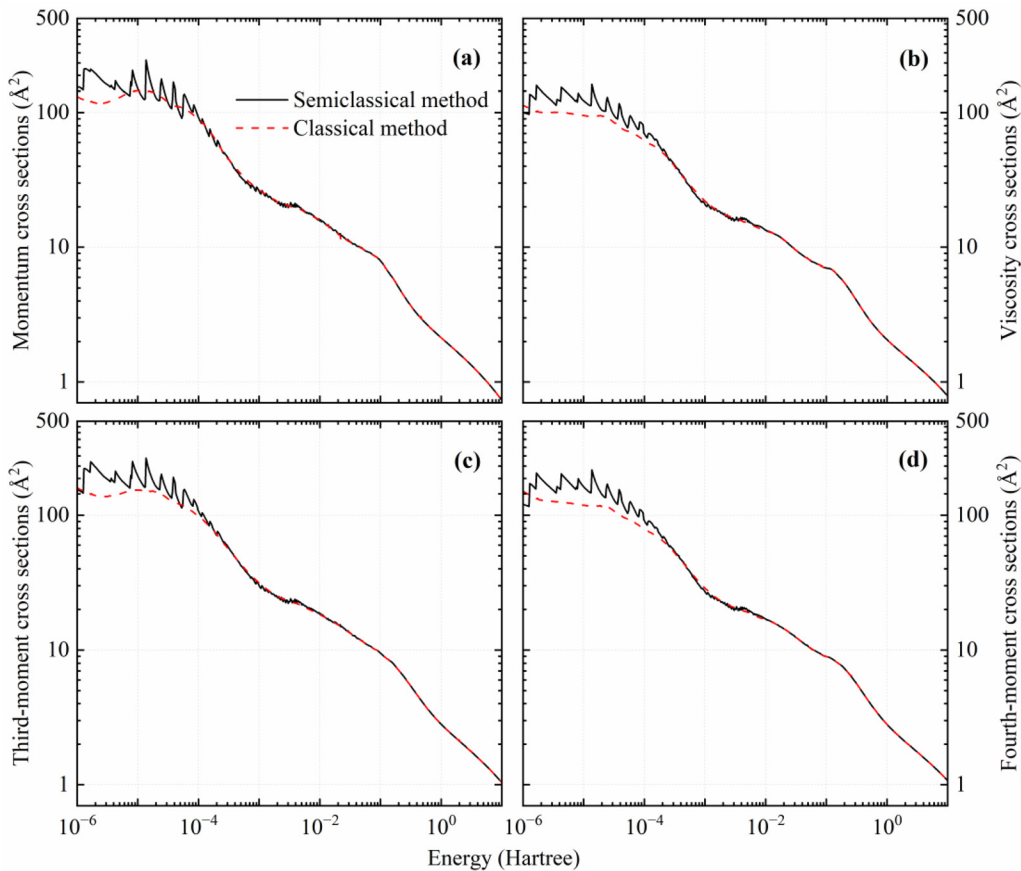


FIG. 5. Transport cross sections including (a) momentum transfer, (b) viscosity, (c) the third-moment, and (d) the fourth-moment cross sections for the $N(^4S)-O(^1D)$ interaction obtained by the semiclassical method and classical method.

TABLE II. Comparison between collision integrals $\sigma^2\Omega^{(1,1)*}$ (in \AA^2) for the $\text{N}^{(4)\text{S}}\text{-O}^{(3)\text{P}}$ interaction calculated in the present work based on classical method (columns a) and semiclassical method (columns b) with those from Levin *et al.*⁹ (columns c), Capitelli *et al.*²³ (columns d), Laricchiuta *et al.*⁴⁹ (columns e), and Yun *et al.*⁴⁸ (columns f).

T (K)	(1,1)a	(1,1)b	(1,1)c	(1,1)d	(1,1)e	(1,1)f
300	8.149	8.173	8.321	8.451	7.855	...
500	7.204	7.210	7.341	7.178	6.952	...
1000	6.164	6.178	6.217	5.788	5.983	7.156
2000	5.265	5.285	5.257	4.626	5.154	5.518
5000	4.130	4.142	4.210	3.343	4.191	4.054
10 000	3.286	3.275	3.439	2.554	3.550	3.246
20 000	2.511	2.487	2.659	1.914	2.984	...
30 000	2.094	2.076	2.240	1.605	2.688	...
50 000	1.618	1.610	1.768	1.276	2.349	...

TABLE III. Comparison between collision integrals $\sigma^2\Omega^{(2,2)*}$ (in \AA^2) for the $\text{N}^{(4)\text{S}}\text{-O}^{(3)\text{P}}$ interaction calculated in the present work based on classical method (columns a) and semiclassical method (columns b) with those from Levin *et al.*⁹ (columns c), Capitelli *et al.*²³ (columns d), Laricchiuta *et al.*⁴⁹ (columns e), and Yun *et al.*⁴⁸ (columns f).

T (K)	(2,2)a	(2,2)b	(2,2)c	(2,2)d	(2,2)e	(2,2)f
300	9.156	9.129	9.078	9.293	8.817	...
500	8.173	8.145	8.152	7.928	7.892	...
1000	7.090	7.076	7.092	6.525	6.893	8.418
2000	6.142	6.136	6.061	5.394	6.011	5.518
5000	4.938	4.935	4.879	4.104	4.947	4.054
10 000	3.983	3.974	4.067	3.242	4.220	3.246
20 000	3.092	3.089	3.208	2.487	3.567	...
30 000	2.620	2.620	2.744	2.101	3.220	...
50 000	2.065	2.065	2.218	1.678	2.822	...

methods, are all close to those from Levin *et al.*⁹ with a deviation of no more than 9.3% over the temperature range of 300–50 000 K. The deviations between our collision integrals and those from Laricchiuta *et al.*⁹ are less than 8% at 300–10 000 K. However, the collision integrals reported by Capitelli *et al.*²³ show a deviation of more than 19% compared to our results and those from Levin *et al.*⁹ at temperatures ranging from 5000 to 50 000 K. Moreover, the results obtained by Laricchiuta *et al.*⁴⁹ deviate by more than 30% from our results and those from Levin *et al.*⁹ at 20 000–50 000 K. For the collision integrals $\sigma^2\Omega^{(2,2)*}$, our results are in good agreement with those from Levin *et al.*⁹ Note that there is a deviation of about 20% between the viscosity-type collision integrals derived from *ab initio* calculation (i.e., our results and those from Levin *et al.*⁹) and those derived from fitting potential energy functions (i.e., the results from Capitelli *et al.*²³ Yun *et al.*⁴⁸ and Laricchiuta *et al.*⁴⁹).

Table IV provides a comparison of collision integrals for $\text{N}^{(4)\text{S}}\text{-O}^{(1)\text{D}}$ interactions with previous theoretical results.⁴⁹ For collision integrals $\sigma^2\Omega^{(1,1)*}$ and $\sigma^2\Omega^{(2,2)*}$, the results present a very good agreement between the classical and semiclassical values. The maximum

TABLE IV. Comparison between collision integrals (in \AA^2) for the $\text{N}^{(4)\text{S}}\text{-O}^{(1)\text{D}}$ interaction calculated in the present work based on the classical method (columns a) and semiclassical method (columns b) with those from Laricchiuta *et al.*⁴⁹ (columns c).

T (K)	(1,1)a	(1,1)b	(1,1)c	(2,2)a	(2,2)b	(2,2)c
300	7.003	7.005	7.931	7.833	7.893	8.885
500	6.249	6.314	7.034	7.091	7.242	7.968
1000	5.313	5.375	6.072	6.198	6.274	6.976
2000	4.373	4.420	5.250	5.165	5.179	6.104
5000	3.348	3.370	4.290	3.922	3.921	5.049
10 000	2.659	2.667	3.650	3.232	3.231	4.325
20 000	1.918	1.920	3.082	2.418	2.418	3.672
30 000	1.528	1.528	2.784	1.931	1.931	3.325
50 000	1.143	1.143	2.442	1.432	1.433	2.924

deviation between classical values and semiclassical values is 2.09% for collision integrals $\sigma^2\Omega^{(2,2)*}$ at 500 K. Note that the deviation between classical and semiclassical values shows non-regular variation with increasing temperature. The deviation of collision integrals is mainly caused by quantum mechanical effects and is concentrated at low temperatures (<1000 K). Theoretically, the results obtained by the semiclassical method may show more accurate collision integrals for N–O interaction. However, the collision integrals obtained by the phenomenological approach⁴⁹ have a large deviation from our results. The deviation is particularly noticeable at high temperatures, with a maximum deviation of 113% observed at 50 000 K for the $\sigma^2\Omega^{(1,1)*}$.

Although the transport cross sections calculated by the classical and semiclassical methods are very different at low collision energies, these differences for cross sections below 10^{-4} Hartree has little effect on the collision integrals above 300 K. Our calculated collision integrals $\sigma^2\Omega^{(1,1)*}$ and $\sigma^2\Omega^{(2,2)*}$ obtained by the classical method are in excellent agreement with those derived from semiclassical methods at 300–50 000 K, with the maximum deviations not exceeding 1%. On the other hand, the deviation of collision integrals caused by using different methods is much smaller than those induced by adopting different forms of PECs for N–O interactions. These deviations are within acceptable limits while ensuring the accuracy of PECs. For N–O interactions, the time required to compute the collision integrals using the semiclassical approach is many times longer than using the classical approach. Considering the computational resources consumed, as well as the deviations induced by these two methods are small and concentrated at low temperatures, the classical method may be more dominant in the modeling of high-temperature plasmas.

Figures 6 and 7 present the collision integrals for $\text{N}^{(4)\text{S}}\text{-O}^{(3)\text{P}}$ and $\text{N}^{(4)\text{S}}\text{-O}^{(1)\text{D}}$ interactions in the temperature range of 300–50 000 K. The deviations of collision integrals based on the classical method and semiclassical method are limited to 0.06\AA^2 for $\text{N}^{(4)\text{S}}\text{-O}^{(3)\text{P}}$ interaction. For $\text{N}^{(4)\text{S}}\text{-O}^{(1)\text{D}}$ interaction, the deviations are mainly concentrated at low temperatures, with deviations within 0.18\AA^2 . The calculated collision integrals include $\sigma^2\Omega^{(1,1)*}$, $\sigma^2\Omega^{(1,2)*}$, $\sigma^2\Omega^{(1,3)*}$, $\sigma^2\Omega^{(1,4)*}$, $\sigma^2\Omega^{(1,5)*}$, $\sigma^2\Omega^{(2,2)*}$, $\sigma^2\Omega^{(2,3)*}$, $\sigma^2\Omega^{(2,4)*}$, $\sigma^2\Omega^{(2,5)*}$, $\sigma^2\Omega^{(2,6)*}$, $\sigma^2\Omega^{(3,3)*}$, and $\sigma^2\Omega^{(4,4)*}$. For more detailed information on the collision integrals, refer to the supplementary material. These results support the calculation of transport coefficients in a third-order approximation. In the Appendix, the fitting functions of collision

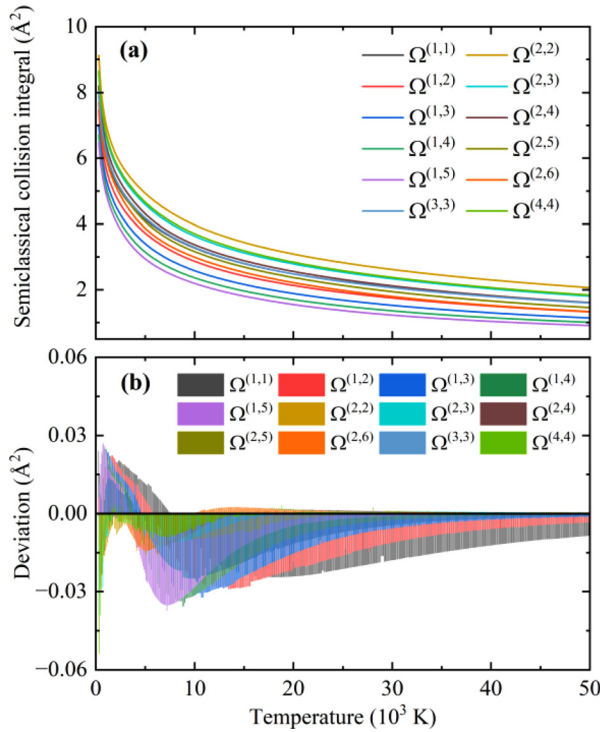


FIG. 6. (a) Semiclassical collision integrals and (b) deviations of collision integrals based on classical method and semiclassical method corresponding to the $N(^4S)-O(^3P)$ interaction as a function of temperature.

integrals for $N(^4S)-O(^3P)$ and $N(^4S)-O(^1D)$ interactions are reported with the following functional forms:

$$f_{\sigma^2\Omega^{(l,s)}}(T) = a_1 + a_2T + a_3T^2 + a_4T^3 + a_5T^4 + a_6T^5 + a_7T^6 + \frac{a_8}{T} + \frac{a_9}{T^2} + \frac{a_{10}}{T^3}, \quad (9)$$

where $a_1, a_2, a_3, a_4, a_5, a_6, a_7, a_8, a_9,$ and a_{10} are the fitting parameters. The fitting errors of collision integrals for $N(^4S)-O(^3P)$ and $N(^4S)-O(^1D)$ interactions relative to the calculated ones are less than 1.2%.

Assuming that the N and O atoms in the plasma mixture are in thermodynamic equilibrium below 20 000 K with only $N(^3P), O(^3P),$ and $O(^1D),$ and that their numbers in the ground and excited states satisfy the Boltzmann distribution equation. We can estimate the proportion of O atoms in the ground and excited states to the total number of O atoms at a temperature of $T,$ ⁵⁰

$$\frac{n_i}{n_{totl}} = \frac{g_i}{Z(T)} \exp\left(-\frac{E_i}{kT}\right), \quad (10)$$

where n_i is the equilibrium population of the i th energy level, g_i is the degeneracy of the i th energy level, E_i is the energy difference between the i th energy level and the ground state atomic oxygen, and $Z(T)$ is the partition function of atomic oxygen. Figure 8 presents the proportion of O atoms in the ground and excited states to the total number of O atoms. Note that the number of O atoms in the first excited state reaches 24% of the total number of O atoms at 20 000 K.

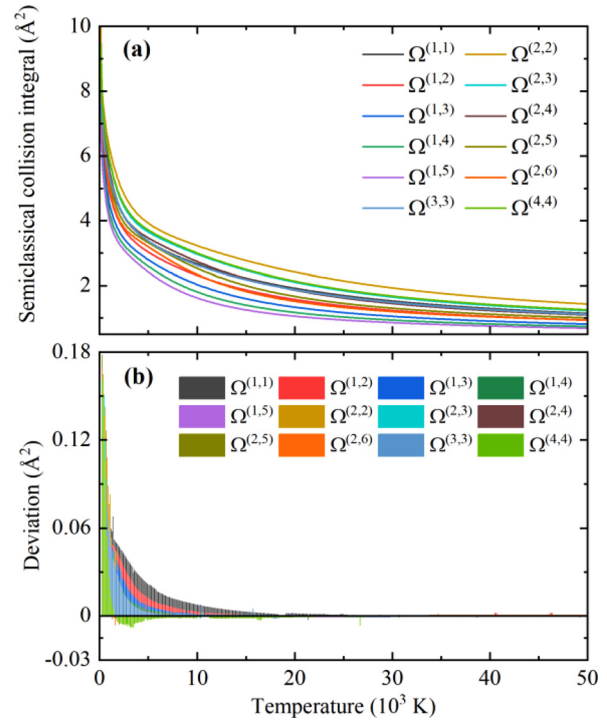


FIG. 7. (a) Semiclassical collision integrals and (b) deviations of collision integrals based on classical method and semiclassical method corresponding to the $N(^4S)-O(^1D)$ interaction as a function of temperature.

We calculate the first-order thermal conductivity λ for a mixture of N and O based on the proportion of O atoms in the ground and excited states to the total number of O atoms, with a mixture ratio of N atoms to O atoms is 1:1. The λ can be obtained from the following relation:⁴

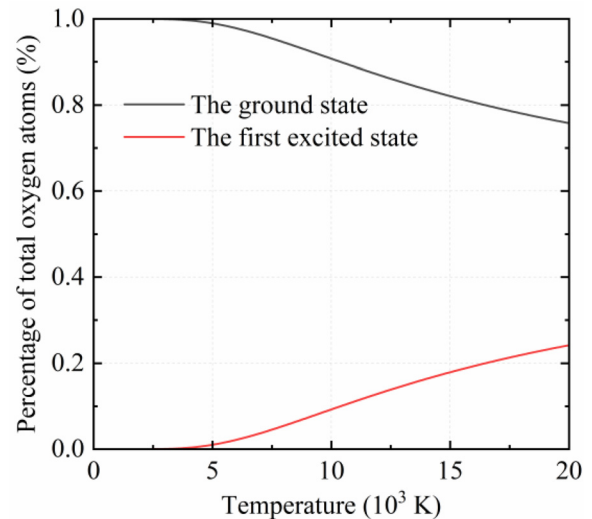


FIG. 8. Oxygen atoms in ground and excited states as a percentage of the total number of oxygen atoms.

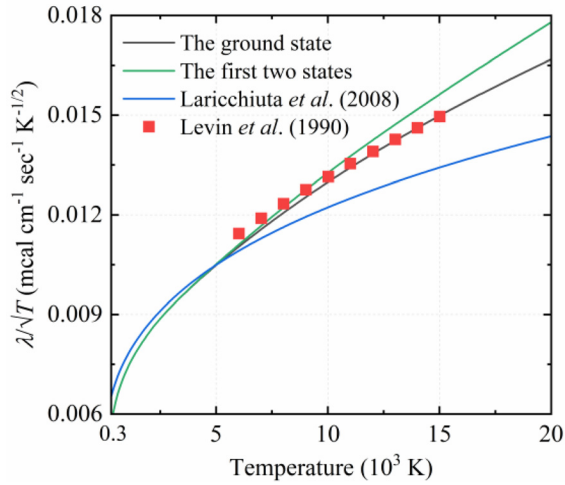


FIG. 9. Comparison between thermal conductivity for N–O interaction calculated in the present work, Laricchiuta *et al.*⁴⁹ and Levin *et al.*⁹

$$[\lambda_{12}]_1 = \frac{25}{32} \frac{\sqrt{(m_1 + m_2)\pi k_B T / 2m_1 m_2}}{\pi \sigma_{12}^2 \Omega_{12}^{(2,2)}} \left(\frac{3}{2} k_B \right), \quad (11)$$

where m_1 and m_2 are the molecular weights of species 1 and 2, respectively.

This calculation is done using collision integrals of $N(^4S)-O(^3P)$ interaction and collision integrals for $N(^4S)-O(^3P)$ and $N(^4S)-O(^1D)$ interactions, as shown in Fig. 9. The λ of Levin *et al.*⁹ were calculated by collision integrals for the $N(^4S)-O(^3P)$ interaction, and those of Laricchiuta *et al.*⁴⁹ were calculated based on collision integrals for $N(^4S)-O(^3P)$ and $N(^4S)-O(^1D)$ interactions. Our calculations show that the maximum deviation of λ from those of Levin *et al.*⁹ is about 3.7% at 6000 K, and this deviation decreases with increasing temperature. The deviation gradually increases with the temperature increases. When considering the $N(^4S)-O(^1D)$ interaction, a difference in thermal conductivity becomes apparent at 5000 K and increases to 6.7% at 20 000 K (see black and green lines in Fig. 9). The results of Laricchiuta *et al.*⁴⁹ agree well with our collision integrals below 5000 K. The collision integrals obtained by Laricchiuta *et al.*⁴⁹ differ significantly from our results at high temperatures (see Tables II–IV). Since the transport coefficients are the linear combination of the collision integrals,⁴ this leads to a large deviation in the calculated transport coefficient, with a maximum deviation of 19% observed at 20 000 K.

IV. CONCLUSIONS

In the present work, we have investigated the momentum transfer, viscosity, third-moment, and fourth-moment transport cross sections for the $N(^4S)-O(^3P)$ and $N(^4S)-O(^1D)$ interactions using the classical and semiclassical methods. The potential energy curves for the N–O interactions are obtained using the icMRCI+Q method with the aug-cc-pV6Z basis set and reasonable extrapolations. We provided the classical and semiclassical collision integrals for the $N(^4S)-O(^3P)$ and $N(^4S)-O(^1D)$ interactions in the temperature range of 300–50 000 K. The transport cross sections and collision integrals for the $N(^4S)-O(^1D)$ interaction are calculated using the *ab initio* potential energy points for the first time. The deviations of results obtained by

classical and semiclassical methods do not exceed 3% and are concentrated at low temperatures. The results support the calculation of the transport coefficients in the third-order approximation, contributing to the development of high-precision reentry models containing nitrogen and oxygen atoms.

SUPPLEMENTARY MATERIAL

See the supplementary material for the *ab initio* potential energy points for the $N(^4S)-O(^3P)$ and $N(^4S)-O(^1D)$ interactions given in $N(^4S)-O(^3P)$ *ab initio* points.txt and $N(^4S)-O(^1D)$ *ab initio* points.txt, the classical and semiclassical collision integrals for the $N(^4S)-O(^3P)$ and $N(^4S)-O(^1D)$ interactions given in $N(^4S)-O(^3P)$ classical collision integrals.txt, $N(^4S)-O(^3P)$ semiclassical collision integrals.txt, $N(^4S)-O(^1D)$ classical collision integrals.txt, and $N(^4S)-O(^1D)$ semiclassical collision integrals.txt.

ACKNOWLEDGMENTS

This work is sponsored by National Natural Science Foundation of China (52106098), Natural Science Foundation of Shandong Province (ZR2021QE021), Postdoctoral Innovation Project of Shandong Province and Postdoctoral Applied Research Project of Qingdao City, and Young Scholars Program of Shandong University. The scientific calculations in this paper have been done on the HPC Cloud Platform of Shandong University.

AUTHOR DECLARATIONS

Conflict of Interest

The authors have no conflicts to disclose.

Author Contributions

Zi Ding: Formal analysis (equal); Investigation (equal); Software (equal); Visualization (equal); Writing – original draft (equal). **Zhi Qin:** Conceptualization (equal); Funding acquisition (equal); Project administration (equal); Resources (equal); Supervision (equal); Writing – review & editing (equal). **Linhua Liu:** Funding acquisition (equal); Project administration (equal); Supervision (equal).

DATA AVAILABILITY

The data that support the findings of this study are available within the article and its supplementary material.

APPENDIX: EXPRESSIONS FOR THE FIRST FOUR-MOMENT TRANSPORT CROSS SECTIONS

The expressions for the first four-moment transport cross sections (MTCSs, VCSs, TCSs, and FCSs) are as follows:

$$Q^{(1)} = \frac{4\pi}{k^2} \sum_{l=0}^{\infty} (l+1) \sin^2(\eta_l - \eta_{l+1}), \quad (A1)$$

$$Q^{(2)} = \frac{4\pi}{k^2} \sum_{l=0}^{\infty} \frac{(l+1)(l+2)}{2l+3} \sin^2(\eta_l - \eta_{l+2}), \quad (A2)$$

TABLE V. The fitting parameters of collision integrals for the $N(^4S)-O(^3P)$ interaction.

Parameters	$\sigma^2\Omega^{(1,1)*}$	$\sigma^2\Omega^{(1,2)*}$	$\sigma^2\Omega^{(1,3)*}$	$\sigma^2\Omega^{(1,4)*}$	$\sigma^2\Omega^{(1,5)*}$	$\sigma^2\Omega^{(2,2)*}$
a_1 (\AA^2)	$5.405\,838\,35 \times 10^{+00}$	$5.083\,206\,01 \times 10^{+00}$	$4.807\,015\,67 \times 10^{+00}$	$4.544\,037\,02 \times 10^{+00}$	$4.299\,184\,80 \times 10^{+00}$	$6.281\,889\,09 \times 10^{+00}$
a_2 ($\text{\AA}^2/\text{K}$)	$-4.282\,138\,41 \times 10^{-04}$	$-4.559\,549\,47 \times 10^{-04}$	$-4.695\,676\,16 \times 10^{-04}$	$-4.668\,698\,72 \times 10^{-04}$	$-4.549\,098\,47 \times 10^{-04}$	$-4.384\,813\,97 \times 10^{-04}$
a_3 ($\text{\AA}^2/\text{K}^2$)	$3.140\,310\,12 \times 10^{-08}$	$3.525\,512\,86 \times 10^{-08}$	$3.780\,520\,21 \times 10^{-08}$	$3.831\,083\,46 \times 10^{-08}$	$3.751\,402\,21 \times 10^{-08}$	$2.928\,012\,84 \times 10^{-08}$
a_4 ($\text{\AA}^2/\text{K}^3$)	$-1.438\,769\,21 \times 10^{-12}$	$-1.664\,411\,21 \times 10^{-12}$	$-1.834\,855\,96 \times 10^{-12}$	$-1.885\,743\,91 \times 10^{-12}$	$-1.854\,478\,93 \times 10^{-12}$	$-1.252\,294\,49 \times 10^{-12}$
a_5 ($\text{\AA}^2/\text{K}^4$)	$3.766\,929\,23 \times 10^{-17}$	$4.438\,098\,13 \times 10^{-17}$	$4.992\,743\,65 \times 10^{-17}$	$5.190\,719\,84 \times 10^{-17}$	$5.130\,239\,61 \times 10^{-17}$	$3.129\,791\,80 \times 10^{-17}$
a_6 ($\text{\AA}^2/\text{K}^5$)	$-5.150\,478\,15 \times 10^{-22}$	$-6.138\,353\,69 \times 10^{-22}$	$-7.010\,311\,92 \times 10^{-22}$	$-7.355\,661\,78 \times 10^{-22}$	$-7.304\,516\,00 \times 10^{-22}$	$-4.150\,269\,01 \times 10^{-22}$
a_7 ($\text{\AA}^2/\text{K}^6$)	$2.845\,976\,02 \times 10^{-27}$	$3.417\,241\,78 \times 10^{-27}$	$3.947\,505\,82 \times 10^{-27}$	$4.172\,285\,05 \times 10^{-27}$	$4.160\,418\,35 \times 10^{-27}$	$2.247\,072\,73 \times 10^{-27}$
a_8 ($\text{\AA}^2 \cdot \text{K}$)	$1.263\,206\,48 \times 10^{+03}$	$1.154\,567\,89 \times 10^{+03}$	$1.125\,468\,05 \times 10^{+03}$	$1.143\,776\,90 \times 10^{+03}$	$1.180\,286\,91 \times 10^{+03}$	$1.330\,496\,43 \times 10^{+03}$
a_9 ($\text{\AA}^2 \cdot \text{K}^2$)	$-1.410\,543\,11 \times 10^{+05}$	$-1.409\,780\,01 \times 10^{+05}$	$-1.466\,936\,84 \times 10^{+05}$	$-1.581\,907\,13 \times 10^{+05}$	$-1.713\,308\,33 \times 10^{+05}$	$-1.509\,547\,22 \times 10^{+05}$
a_{10} ($\text{\AA}^2 \cdot \text{K}^3$)	$7.528\,645\,28 \times 10^{+06}$	$7.508\,419\,71 \times 10^{+06}$	$7.850\,062\,78 \times 10^{+06}$	$8.560\,108\,65 \times 10^{+06}$	$9.377\,034\,68 \times 10^{+06}$	$8.137\,525\,09 \times 10^{+06}$
Parameters	$\sigma^2\Omega^{(2,3)*}$	$\sigma^2\Omega^{(2,4)*}$	$\sigma^2\Omega^{(2,5)*}$	$\sigma^2\Omega^{(2,6)*}$	$\sigma^2\Omega^{(3,3)*}$	$\sigma^2\Omega^{(4,4)*}$
a_1 (\AA^2)	$6.075\,398\,57 \times 10^{+00}$	$5.915\,637\,62 \times 10^{+00}$	$5.756\,638\,98 \times 10^{+00}$	$5.597\,729\,45 \times 10^{+00}$	$5.537\,549\,34 \times 10^{+00}$	$6.154\,683\,50 \times 10^{+00}$
a_2 ($\text{\AA}^2/\text{K}$)	$-4.769\,133\,12 \times 10^{-04}$	$-5.160\,566\,14 \times 10^{-04}$	$-5.445\,872\,38 \times 10^{-04}$	$-5.633\,443\,22 \times 10^{-04}$	$-4.428\,119\,18 \times 10^{-04}$	$-4.790\,304\,89 \times 10^{-04}$
a_3 ($\text{\AA}^2/\text{K}^2$)	$3.357\,138\,52 \times 10^{-08}$	$3.871\,042\,56 \times 10^{-08}$	$4.301\,421\,43 \times 10^{-08}$	$4.630\,898\,59 \times 10^{-08}$	$3.197\,000\,69 \times 10^{-08}$	$3.378\,246\,92 \times 10^{-08}$
a_4 ($\text{\AA}^2/\text{K}^3$)	$-1.467\,151\,64 \times 10^{-12}$	$-1.761\,703\,06 \times 10^{-12}$	$-2.029\,104\,87 \times 10^{-12}$	$-2.249\,860\,87 \times 10^{-12}$	$-1.453\,678\,75 \times 10^{-12}$	$-1.486\,247\,18 \times 10^{-12}$
a_5 ($\text{\AA}^2/\text{K}^4$)	$3.687\,272\,54 \times 10^{-17}$	$4.542\,890\,74 \times 10^{-17}$	$5.363\,776\,49 \times 10^{-17}$	$6.077\,077\,73 \times 10^{-17}$	$3.803\,634\,64 \times 10^{-17}$	$3.761\,124\,82 \times 10^{-17}$
a_6 ($\text{\AA}^2/\text{K}^5$)	$-4.880\,244\,05 \times 10^{-22}$	$-6.112\,754\,30 \times 10^{-22}$	$-7.342\,923\,89 \times 10^{-22}$	$-8.452\,510\,02 \times 10^{-22}$	$-5.213\,119\,53 \times 10^{-22}$	$-5.006\,532\,07 \times 10^{-22}$
a_7 ($\text{\AA}^2/\text{K}^6$)	$2.629\,152\,55 \times 10^{-27}$	$3.329\,108\,65 \times 10^{-27}$	$4.048\,492\,63 \times 10^{-27}$	$4.716\,043\,79 \times 10^{-27}$	$2.890\,181\,80 \times 10^{-27}$	$2.709\,193\,53 \times 10^{-27}$
a_8 ($\text{\AA}^2 \cdot \text{K}$)	$1.206\,559\,76 \times 10^{+03}$	$1.122\,724\,71 \times 10^{+03}$	$1.083\,960\,65 \times 10^{+03}$	$1.074\,875\,91 \times 10^{+03}$	$1.232\,005\,21 \times 10^{+03}$	$1.215\,306\,41 \times 10^{+03}$
a_9 ($\text{\AA}^2 \cdot \text{K}^2$)	$-1.406\,915\,97 \times 10^{+05}$	$-1.325\,721\,04 \times 10^{+05}$	$-1.316\,589\,29 \times 10^{+05}$	$-1.358\,378\,38 \times 10^{+05}$	$-1.518\,334\,63 \times 10^{+05}$	$-1.434\,814\,34 \times 10^{+05}$
a_{10} ($\text{\AA}^2 \cdot \text{K}^3$)	$7.400\,452\,39 \times 10^{+06}$	$6.860\,441\,80 \times 10^{+06}$	$6.815\,973\,67 \times 10^{+06}$	$7.110\,887\,12 \times 10^{+06}$	$8.183\,949\,06 \times 10^{+06}$	$7.560\,168\,35 \times 10^{+06}$

TABLE VI. The fitting parameters of collision integrals for $N(^4S)-O(^1D)$ interaction.

Parameters	$\sigma^2\Omega^{(1,1)*}$	$\sigma^2\Omega^{(1,2)*}$	$\sigma^2\Omega^{(1,3)*}$	$\sigma^2\Omega^{(1,4)*}$	$\sigma^2\Omega^{(1,5)*}$	$\sigma^2\Omega^{(2,2)*}$
a_1 (\AA^2)	$5.451\,572\,84 \times 10^{+00}$	$5.155\,238\,12 \times 10^{+00}$	$4.908\,984\,74 \times 10^{+00}$	$4.655\,645\,57 \times 10^{+00}$	$4.407\,840\,17 \times 10^{+00}$	$6.317\,923\,62 \times 10^{+00}$
a_2 ($\text{\AA}^2/\text{K}$)	$-4.321\,839\,72 \times 10^{-04}$	$-4.712\,837\,53 \times 10^{-04}$	$-4.999\,849\,72 \times 10^{-04}$	$-5.067\,752\,32 \times 10^{-04}$	$-4.996\,277\,60 \times 10^{-04}$	$-4.474\,150\,06 \times 10^{-04}$
a_3 ($\text{\AA}^2/\text{K}^2$)	$3.085\,706\,67 \times 10^{-08}$	$3.590\,019\,42 \times 10^{-08}$	$4.050\,248\,42 \times 10^{-08}$	$4.260\,762\,38 \times 10^{-08}$	$4.291\,060\,96 \times 10^{-08}$	$2.997\,101\,86 \times 10^{-08}$
a_4 ($\text{\AA}^2/\text{K}^3$)	$-1.378\,397\,76 \times 10^{-12}$	$-1.656\,513\,43 \times 10^{-12}$	$-1.946\,160\,63 \times 10^{-12}$	$-2.101\,981\,16 \times 10^{-12}$	$-2.153\,011\,37 \times 10^{-12}$	$-1.273\,983\,40 \times 10^{-12}$
a_5 ($\text{\AA}^2/\text{K}^4$)	$3.545\,046\,40 \times 10^{-17}$	$4.329\,836\,28 \times 10^{-17}$	$5.229\,502\,74 \times 10^{-17}$	$5.757\,357\,99 \times 10^{-17}$	$5.977\,368\,26 \times 10^{-17}$	$3.153\,699\,94 \times 10^{-17}$
a_6 ($\text{\AA}^2/\text{K}^5$)	$-4.789\,705\,24 \times 10^{-22}$	$-5.895\,848\,56 \times 10^{-22}$	$-7.260\,131\,99 \times 10^{-22}$	$-8.105\,691\,18 \times 10^{-22}$	$-8.504\,522\,58 \times 10^{-22}$	$-4.140\,823\,64 \times 10^{-22}$
a_7 ($\text{\AA}^2/\text{K}^6$)	$2.625\,565\,58 \times 10^{-27}$	$3.243\,073\,49 \times 10^{-27}$	$4.049\,754\,15 \times 10^{-27}$	$4.568\,862\,40 \times 10^{-27}$	$4.833\,085\,34 \times 10^{-27}$	$2.221\,846\,42 \times 10^{-27}$
a_8 ($\text{\AA}^2 \cdot \text{K}$)	$1.225\,162\,90 \times 10^{+03}$	$1.103\,324\,95 \times 10^{+03}$	$1.061\,334\,37 \times 10^{+03}$	$1.082\,715\,91 \times 10^{+03}$	$1.129\,841\,93 \times 10^{+03}$	$1.276\,920\,31 \times 10^{+03}$
a_9 ($\text{\AA}^2 \cdot \text{K}^2$)	$-1.297\,091\,72 \times 10^{+05}$	$-1.297\,051\,81 \times 10^{+05}$	$-1.338\,763\,55 \times 10^{+05}$	$-1.473\,089\,46 \times 10^{+05}$	$-1.634\,431\,79 \times 10^{+05}$	$-1.381\,723\,12 \times 10^{+05}$
a_{10} ($\text{\AA}^2 \cdot \text{K}^3$)	$6.935\,051\,38 \times 10^{+06}$	$6.930\,293\,57 \times 10^{+06}$	$7.177\,489\,37 \times 10^{+06}$	$7.999\,486\,50 \times 10^{+06}$	$9.002\,315\,55 \times 10^{+06}$	$7.541\,745\,76 \times 10^{+06}$
Parameters	$\sigma^2\Omega^{(2,3)*}$	$\sigma^2\Omega^{(2,4)*}$	$\sigma^2\Omega^{(2,5)*}$	$\sigma^2\Omega^{(2,6)*}$	$\sigma^2\Omega^{(3,3)*}$	$\sigma^2\Omega^{(4,4)*}$
a_1 (\AA^2)	$6.127\,268\,04 \times 10^{+00}$	$5.959\,120\,93 \times 10^{+00}$	$5.794\,242\,93 \times 10^{+00}$	$5.618\,500\,32 \times 10^{+00}$	$5.632\,873\,48 \times 10^{+00}$	$6.195\,827\,71 \times 10^{+00}$
a_2 ($\text{\AA}^2/\text{K}$)	$-4.942\,079\,12 \times 10^{-04}$	$-5.336\,117\,49 \times 10^{-04}$	$-5.620\,554\,37 \times 10^{-04}$	$-5.763\,816\,67 \times 10^{-04}$	$-4.717\,252\,46 \times 10^{-04}$	$-4.940\,911\,12 \times 10^{-04}$
a_3 ($\text{\AA}^2/\text{K}^2$)	$3.554\,928\,73 \times 10^{-08}$	$4.098\,803\,29 \times 10^{-08}$	$4.549\,213\,57 \times 10^{-08}$	$4.837\,733\,13 \times 10^{-08}$	$3.476\,587\,92 \times 10^{-08}$	$3.569\,393\,73 \times 10^{-08}$
a_4 ($\text{\AA}^2/\text{K}^3$)	$-1.572\,736\,44 \times 10^{-12}$	$-1.895\,245\,48 \times 10^{-12}$	$-2.184\,354\,71 \times 10^{-12}$	$-2.387\,802\,81 \times 10^{-12}$	$-1.583\,563\,43 \times 10^{-12}$	$-1.598\,257\,61 \times 10^{-12}$
a_5 ($\text{\AA}^2/\text{K}^4$)	$3.977\,765\,03 \times 10^{-17}$	$4.938\,316\,93 \times 10^{-17}$	$5.848\,142\,49 \times 10^{-17}$	$6.525\,214\,81 \times 10^{-17}$	$4.123\,343\,98 \times 10^{-17}$	$4.094\,989\,98 \times 10^{-17}$
a_6 ($\text{\AA}^2/\text{K}^5$)	$-5.280\,412\,91 \times 10^{-22}$	$-6.690\,758\,57 \times 10^{-22}$	$-8.081\,664\,08 \times 10^{-22}$	$-9.155\,591\,32 \times 10^{-22}$	$-5.615\,357\,35 \times 10^{-22}$	$-5.498\,986\,22 \times 10^{-22}$
a_7 ($\text{\AA}^2/\text{K}^6$)	$2.847\,877\,01 \times 10^{-27}$	$3.660\,868\,15 \times 10^{-27}$	$4.487\,727\,34 \times 10^{-27}$	$5.142\,840\,85 \times 10^{-27}$	$3.094\,031\,89 \times 10^{-27}$	$2.994\,595\,62 \times 10^{-27}$
a_8 ($\text{\AA}^2 \cdot \text{K}$)	$1.153\,969\,87 \times 10^{+03}$	$1.087\,558\,48 \times 10^{+03}$	$1.060\,874\,24 \times 10^{+03}$	$1.067\,232\,17 \times 10^{+03}$	$1.157\,987\,70 \times 10^{+03}$	$1.172\,811\,44 \times 10^{+03}$
a_9 ($\text{\AA}^2 \cdot \text{K}^2$)	$-1.316\,390\,29 \times 10^{+05}$	$-1.286\,510\,55 \times 10^{+05}$	$-1.309\,075\,89 \times 10^{+05}$	$-1.381\,803\,28 \times 10^{+05}$	$-1.375\,409\,61 \times 10^{+05}$	$-1.379\,877\,01 \times 10^{+05}$
a_{10} ($\text{\AA}^2 \cdot \text{K}^3$)	$7.099\,425\,74 \times 10^{+06}$	$6.831\,213\,62 \times 10^{+06}$	$6.941\,824\,79 \times 10^{+06}$	$7.381\,583\,33 \times 10^{+06}$	$7.448\,024\,77 \times 10^{+06}$	$7.419\,317\,63 \times 10^{+06}$

$$Q^{(3)} = \frac{4\pi}{k^2} \sum_{l=0}^{\infty} \frac{l+1}{2l+5} \left[\frac{3(l^2+2l-1)}{2l-1} \sin^2(\eta_l - \eta_{l+1}) + \frac{(l+2)(l+3)}{2l+3} \sin^2(\eta_l - \eta_{l+3}) \right], \quad (\text{A3})$$

$$Q^{(4)} = \frac{4\pi}{k^2} \sum_{l=0}^{\infty} \frac{(l+1)(l+2)}{(2l+3)(2l+7)} \left[\frac{2(2l^2+6l-3)}{2l-1} \sin^2(\eta_l - \eta_{l+2}) + \frac{(l+3)(l+4)}{2l+5} \sin^2(\eta_l - \eta_{l+4}) \right]. \quad (\text{A4})$$

Tables V and VI present the parameters for fitting functions of collision integrals for $\text{N}^{(4)\text{S}}\text{-O}^{(3)\text{P}}$ and $\text{N}^{(4)\text{S}}\text{-O}^{(1)\text{D}}$ interactions.

REFERENCES

- ¹T. K. Mankodi, U. V. Bhandarkar, and R. S. Myong, "Collision cross sections and nonequilibrium viscosity coefficients of N_2 and O_2 based on molecular dynamics," *Phys. Fluids* **32**, 036102 (2020).
- ²L. A. Nicasio-Collazo, C. A. Ramírez-Medina, and A. Torres-Carbajal, "Dynamical behavior and transport coefficients of the pseudo hard-sphere fluid," *Phys. Fluids* **35**, 087118 (2023).
- ³D. Zhang, A. Xu, Y. Gan, Y. Zhang, J. Song, and Y. Li, "Viscous effects on morphological and thermodynamic non-equilibrium characterizations of shock-bubble interaction," *Phys. Fluids* **35**, 106113 (2023).
- ⁴J. O. Hirschfelder, C. F. Curtiss, and R. B. Bird, *Molecular Theory of Gases and Liquids* (John Wiley & Sons, 1964).
- ⁵S. Chapman and T. G. Cowling, *The Mathematical Theory of Non-Uniform Gases: An account of the Kinetic Theory of Viscosity, Thermal Conduction and Diffusion in Gases* (Cambridge University Press, 1990).
- ⁶E. Levin and M. J. Wright, "Collision integrals for ion-neutral interactions of nitrogen and oxygen," *J. Thermophys. Heat Transfer* **18**, 143 (2004).
- ⁷X. Wang, J. Guo, Q. Hong, and S. Li, "High-fidelity state-to-state modeling of hypersonic flow over a double cone," *Phys. Fluids* **35**, 116101 (2023).
- ⁸A. Appar, A. Bajpai, U. K. Sivakumar, S. K. Naspoori, and R. Kumar, "Rarefied gas effects on hypersonic flow over a transpiration-cooled flat plate," *Phys. Fluids* **35**, 16109 (2023).
- ⁹E. Levin, H. Partridge, and J. R. Stallcop, "Collision integrals and high temperature transport properties for N-N, O-O, and N-O," *J. Thermophys. Heat Transfer* **4**, 469 (1990).
- ¹⁰V. A. Krasnopolsky, "A sensitive search for nitric oxide in the lower atmospheres of Venus and Mars: Detection on Venus and upper limit for Mars," *Icarus* **182**, 80 (2006).
- ¹¹J. Gérard, B. Hubert, J. Gustin, V. I. Shematovich, D. Bisikalo, G. R. Gladstone, and L. W. Esposito, "EUV spectroscopy of the Venus dayglow with UVIS on Cassini," *Icarus* **211**, 70 (2011).
- ¹²P. D. Feldman, E. B. Burgh, S. T. Durrance, and A. F. Davidsen, "Far-ultraviolet spectroscopy of Venus and Mars at 4 Å resolution with the Hopkins Ultraviolet Telescope on Astro-2," *Astrophys. J.* **538**, 395 (2000).
- ¹³J. Bertaux, F. Leblanc, S. Perrier, E. Quémerais, O. Korabiev, E. Dimarellis, A. Reberac, F. Forget, P. C. Simon, and S. A. Stern, "Nightglow in the upper atmosphere of Mars and implications for atmospheric transport," *Science* **307**, 566 (2005).
- ¹⁴J. Bertaux, B. Gondet, F. Lefèvre, J. Bibring, and F. Montmessin, "First detection of O_2 1.27 μm nightglow emission at Mars with OMEGA/MEX and comparison with general circulation model predictions," *J. Geophys. Res.* **117**, E00J04, <https://doi.org/10.1029/2011JE003890> (2012).
- ¹⁵J. L. Fox and A. Dalgarno, "The production of nitrogen atoms on Mars and their escape," *Planet Space Sci.* **28**, 41 (1980).
- ¹⁶C. Sagan, P. L. Hanst, and A. T. Young, "Nitrogen oxides on Mars," *Planet Space Sci.* **13**, 73 (1965).
- ¹⁷A. Sánchez Lavega, R. Hueso, G. Piccioni, P. Drossart, J. Peralta, S. Pérez Hoyos, C. F. Wilson, F. W. Taylor, K. H. Baines, and D. Luz, "Variable winds on Venus mapped in three dimensions," *Geophys. Res. Lett.* **35**, L13204, <https://doi.org/10.1029/2008GL033817> (2008).
- ¹⁸A. Laricchiuta, D. Bruno, M. Capitelli, C. Catalfamo, R. Celiberto, G. Colonna, P. Diomede, D. Giordano, C. Gorse, and S. Longo, "High temperature Mars atmosphere. Part I: Transport cross sections," *Eur. Phys. J. D* **54**, 607 (2009).
- ¹⁹D. Bruno, C. Catalfamo, M. Capitelli, G. Colonna, O. D. Pascale, P. Diomede, C. Gorse, A. Laricchiuta, S. Longo, and D. Giordano, "Transport properties of high-temperature Jupiter atmosphere components," *Phys. Plasmas* **17**, 112315 (2010).
- ²⁰A. D'Angola, G. Colonna, C. Gorse, and M. Capitelli, "Thermodynamic and transport properties in equilibrium air plasmas in a wide pressure and temperature range," *Eur. Phys. J. D* **46**, 129 (2008).
- ²¹Z. Ding, Z. Qin, and L. Liu, "Collision integrals for $\text{N}^{(4)\text{S}}\text{-N}^{(4)\text{S}}$, $\text{N}^{(4)\text{S}}\text{-N}^{(2)\text{D}}$, and $\text{N}^{(4)\text{S}}\text{-N}^{(2)\text{P}}$ interactions," *Phys. Fluids* **35**, 27127 (2023).
- ²²M. Buchowiecki and P. Szabó, "N-H collision integrals with study of repulsive interactions," *Plasma Sources Sci. Technol.* **31**, 45010 (2022).
- ²³M. Capitelli, C. Gorse, S. Longo, and D. Giordano, "Collision integrals of high-temperature air species," *J. Thermophys. Heat Transfer* **14**, 259 (2000).
- ²⁴M. Capitelli, D. Bruno, and A. Laricchiuta, *Fundamental Aspects of Plasma Chemical Physics: Transport* (Springer Science & Business Media, 2013).
- ²⁵B. Sourd, J. Aubreton, M. Elchinger, M. Labrot, and U. Michon, "High temperature transport coefficients in e/C/H/N/O mixtures," *J. Phys. D* **39**, 1105 (2006).
- ²⁶A. Laricchiuta, G. Colonna, D. Bruno, R. Celiberto, C. Gorse, F. Pirani, and M. Capitelli, "Classical transport collision integrals for a Lennard-Jones like phenomenological model potential," *Chem. Phys. Lett.* **445**, 133 (2007).
- ²⁷M. Su, X. Shen, H. Wang, H. Zhang, Y. Yuan, and Y. An, "Collision integral of nitrogen and oxygen and application to artificially triggered lightning," *Chem. Phys. Lett.* **826**, 140664 (2023).
- ²⁸Z. Ding, Z. Qin, M. Buchowiecki, and L. Liu, "Scattering cross sections and collision integrals for $\text{N}^{(4)\text{S}}\text{-N}^{(3)\text{P}}$ and $\text{N}^{(4)\text{S}}\text{-N}^{(1)\text{D}}$ interactions," *Phys. Fluids* **35**, 087120 (2023).
- ²⁹M. Buchowiecki and P. Szabó, "Collision integrals for nitrogen and hydrogen ionized gas: The exact values and assessment of approximations," *Plasma Chem. Plasma Process.* **43**, 449 (2023).
- ³⁰Z. Hou, Z. Qin, and L. Liu, "Transport cross sections and collision integrals for $\text{C}^{(2)\text{P}}\text{-H}^{(2)\text{S}}$, $\text{C}^{(3)\text{P}}\text{-H}^{(1)\text{S}}$, $\text{C}^{(1)\text{D}}\text{-H}^{(1)\text{S}}$, and $\text{C}^{(4)\text{P}}\text{-H}^{(2)\text{S}}$ interactions," *Phys. Fluids* **35**, 107139 (2023).
- ³¹E. Levin, H. Partridge, and J. Stallcop, "High temperature transport properties of air: N-O interaction energies and collision integrals," AIAA Paper No. 88-2660, June 1988.
- ³²Y. Wu, J. G. Wang, P. S. Krstic, and R. K. Janev, "Oscillation structures in elastic and electron capture cross sections for $\text{H}^+\text{-H}$ collisions in Debye plasmas," *J. Phys. B* **43**, 201003 (2010).
- ³³J. R. Stallcop, H. Partridge, and E. Levin, "Resonance charge transfer, transport cross sections, and collision integrals for $\text{N}^{(3)\text{P}}\text{-N}^{(4)\text{S}}$ and $\text{O}^{(4)\text{S}}\text{-O}^{(2)\text{P}}$ interactions," *J. Chem. Phys.* **95**, 6429 (1991).
- ³⁴G. Heiche and E. A. Mason, "Ion mobilities with charge exchange," *J. Chem. Phys.* **53**, 4687 (1970).
- ³⁵F. R. Meeks, T. J. Cleland, K. E. Hutchinson, and W. L. Taylor, "On the quantum cross sections in dilute gases," *J. Chem. Phys.* **100**, 3813 (1994).
- ³⁶M. Capitelli and R. S. Devoto, "Transport coefficients of high-temperature nitrogen," *Phys. Fluids* **16**, 1835 (1973).
- ³⁷E. Levin, D. W. Schwenke, J. R. Stallcop, and H. Partridge, "Comparison of semi-classical and quantum-mechanical methods for the determination of transport cross sections," *Chem. Phys. Lett.* **227**, 669 (1994).
- ³⁸H. Knof, E. A. Mason, and J. T. Vanderslice, "Interaction energies, charge exchange cross sections, and diffusion cross sections for $\text{N}^+\text{-N}$ and $\text{O}^+\text{-O}$ collisions," *J. Chem. Phys.* **40**, 3548 (1964).
- ³⁹H. J. Werner, P. J. Knowles, G. Knizia, F. R. Manby, M. Schütz, P. Celani, W. Goryffo, D. Kats, T. Korona, and R. Lindh, *MOLPRO, Version 2015.1, A Package of Ab Initio Programs* (University of Cardiff Chemistry Consultants, Cardiff, Wales, UK, 2015).
- ⁴⁰H. J. Werner, P. J. Knowles, G. Knizia, F. R. Manby, and M. Schütz, "Molpro: A general-purpose quantum chemistry program package," *WIREs Comput. Mol. Sci.* **2**, 242 (2012).
- ⁴¹H. Werner, P. J. Knowles, F. R. Manby, J. A. Black, K. Doll, A. Heßelmann, D. Kats, A. Köhn, T. Korona, and D. A. Kreplin, "The Molpro quantum chemistry package," *J. Chem. Phys.* **152**, 144107 (2020).
- ⁴²P. J. Knowles and H. Werner, "An efficient method for the evaluation of coupling coefficients in configuration interaction calculations," *Chem. Phys. Lett.* **145**, 514 (1988).

- ⁴³T. Van Mourik, A. K. Wilson, and T. H. Dunning, Jr., “Benchmark calculations with correlated molecular wavefunctions. XIII. Potential energy curves for He₂, Ne₂ and Ar₂ using correlation consistent basis sets through augmented sextuple zeta,” *Mol. Phys.* **96**, 529 (1999).
- ⁴⁴D. E. Woon and T. H. Dunning, Jr., “Gaussian basis sets for use in correlated molecular calculations. V. Core-valence basis sets for boron through neon,” *J. Chem. Phys.* **103**, 4572 (1995).
- ⁴⁵D. E. Woon and T. H. Dunning, Jr., “Gaussian basis sets for use in correlated molecular calculations. III. The atoms aluminum through argon,” *J. Chem. Phys.* **98**, 1358 (1993).
- ⁴⁶M. C. Zammit, J. A. Leiding, J. Colgan, W. Even, C. J. Fontes, and E. Timmermans, “A comprehensive study of the radiative properties of NO—A first step toward a complete air opacity,” *J. Phys. B* **55**, 184002 (2022).
- ⁴⁷R. J. Le Roy, “LEVEL: A computer program for solving the radial Schrödinger equation for bound and quasibound levels,” *J. Quant. Spectrosc. Radiat. Transfer* **186**, 167 (2017).
- ⁴⁸K. S. Yun and E. A. Mason, “Collision integrals for the transport properties of dissociating air at high temperatures,” *Phys. Fluids* **5**, 380 (1962).
- ⁴⁹A. Laricchiuta, M. Capitelli, D. Bruno, F. Pirani, G. Colonna, C. Gorse, R. Celiberto, C. Catalfamo, and G. Terlizzi, “The role of electronically excited states on transport properties of air plasmas,” AIAA Paper No. 2008-4363, 2008.
- ⁵⁰Y. Li, Y. Wang, D. F. Davidson, and R. K. Hanson, “Collisional excitation kinetics for O(3s⁵S^o) and O(3p⁵P₃) states using laser absorption spectroscopy in shock-heated weakly ionized O₂-Ar mixture,” *Phys. Rev. E* **103**, 063211 (2021).